

Self-Supervised Visual Attention Learning for Vehicle Re-Identification

Ming Li, Yiming Zhao, Yecheng Lyu, Ziming Zhang

Worcester Polytechnic Institute
mli12@wpi.edu

Abstract

Visual attention learning (VAL) aims to produce a confidence map as weights to detect discriminative features in each image for certain task such as vehicle re-identification (ReID) where the same vehicle instance needs to be identified across different cameras. In contrast to the literature, in this paper we propose utilizing self-supervised learning to regularize VAL to improving the performance for vehicle ReID. Mathematically using lifting we can factorize the two functions of VAL and self-supervised regularization through another shared function. We implement such factorization using a deep learning framework consisting of three branches: (1) a global branch as backbone for image feature extraction, (2) an attentional branch for producing attention masks, and (3) a self-supervised branch for regularizing the attention learning. Our network design naturally leads to an end-to-end multi-task joint optimization. We conduct comprehensive experiments on three benchmark datasets for vehicle ReID, *i.e.*, VeRi-776, CityFlow-ReID, and VehicleID. We demonstrate the state-of-the-art (SOTA) performance of our approach with the capability of capturing informative vehicle parts with no corresponding manual labels. We also demonstrate the good generalization of our approach in other ReID tasks such as person ReID and multi-target multi-camera tracking.

1 Introduction

Vehicle ReID is a fundamental and challenging problem in video surveillance, because of little discrepancy among the vehicles from identical make and large variations across images of the same instance. The success of recent works suggests that the key to solve this problem is to incorporate explicit mechanisms to discover and concentrate on informative vehicel parts (*e.g.*, wheels, license plate) in addition to capturing robust features from holistic images. They all struggled, however, to annotate original datasets to provide a variety of supervision for training powerful deep convolutional neural networks (CNNs) using, for instance, view segmentation (Meng et al. 2020), keypoints (Khorramshahi et al. 2019; Wang et al. 2017), orientations (Khorramshahi et al. 2019; Wang et al. 2017; Chu et al. 2019) and key parts (He et al. 2019). These annotation processes involve intensive human efforts, and thus significantly restrict the applicability of such approaches.

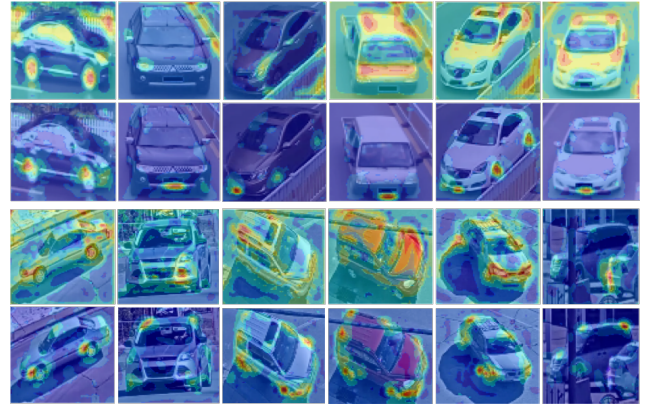


Figure 1: Visual attention mask comparison between (1st & 3rd rows) conventional approach and (2nd & 4th rows) our approach with self-supervised regularization. Our learned masks more focus on the semantic parts of foreground objects, leading to better discriminative features for ReID. Note that our masks are learned with no extra part labels.

Visual Attention Learning (VAL). As a useful alternative to avoid manually labeling in computer vision, various VAL approaches such as channel attention (Hu, Shen, and Sun 2018), spatial attention (Woo et al. 2018) and self-attention (Vaswani et al. 2017) have been proposed and demonstrated to be effective in many vision tasks (Fu et al. 2019; Chen et al. 2019a; Khorramshahi et al. 2019; Chen et al. 2019c). For instance, in spatial attention (Woo et al. 2018) the pooling operation is applied to squeeze channel dimension, followed by a convolutional operation on the 2D spatial features, to output attention maps. Intuitively such approaches are advocated in detecting discriminative features to help improve the performance. However, the output attention masks may be too vague to be understandable of why such masks can help improve the performance.

Self-Supervised Learning (SSL). SSL attempts to learn deep representations by exploring intrinsic properties of data (Jing and Tian 2020), and thus provides supervision enhancement to facilitate the learning of downstream tasks. Some works treated SSL as one branch in the multi-task

scheme to boost the performance of the other task. For example, Gidaris et al. (2019) employed SSL as the auxiliary optimization task of few-shot learning to regularize the shared feature encoder. In the literature of unsupervised learning, similar methods also appeared in, *e.g.*, (Chen et al. 2019d), to provide extra supervision for learning the discriminator, which was demonstrated to stabilize the training of GANs effectively.

Proposed Approach & Contributions. Motivated by recent works in VAL and SSL, we propose an SSL approach as regularization for VAL to learn attention masks with no extra human labels. Fig. 1 illustrates the differences in the attention masks learned with or without SSL regularization for vehicle ReID. As we see clearly, the attention masks learned with SSL regularization more focus on the critical vehicle parts such as license plate, wheels and corners of vehicle top that can potentially lead to unique features for identifying the instances across not only different cameras but also multiple views (*e.g.*, images with rotations). Conceptually this behavior does make sense, because in order to identify the vehicles from the same make, for instance, successfully detecting such distinguishing parts on the vehicles is the key to solving vehicle ReID.

To regularize VAL in a principle way, mathematically using lifting we factorize the two functions of VAL and self-supervised regularization through another shared function. As an effective instantiation, we propose a deep learning framework to learn discriminative features with attention for ReID tasks, as illustrated in Fig. 2. Our framework consists of three branches, *i.e.*, a global branch as backbone for image feature extraction, an attentional branch for producing attention masks, and a self-supervised branch for regularizing the attention learning by sharing the weights with the attentional branch. Each branch introduces its own loss for training the network, and at test time only the global and attentional branches are activated for vehicle ReID.

In summary, the contributions of our paper are as follows:

- We propose regularizing the visual attention learning using self-supervised learning through lifting. To the best of our knowledge, we are the *first* to propose such learning mechanism in the literature of visual attention learning.
- We propose a novel network architecture for ReID tasks to generate physically interpretable attention masks as well as improve the performance with discriminative features.
- We demonstrate the SOTA performance for vehicle ReID on VeRi-776 (Liu et al. 2016b), CityFlow-ReID (Tang et al. 2019b) and VehicleID (Liu et al. 2016a).

2 Related Works

Vehicle ReID. Most of existing works aimed to exploit extra annotations to supervise ReID feature learning. These works can be grouped into three mainstreams as follows: (1) adopting attribute labels (*e.g.*, color and model) (Guo et al. 2019; Yan et al. 2017; Liu et al. 2017, 2016b, 2018; Zhou and Shao 2018) or temporal information (Wang et al. 2017; Shen et al. 2017) to regularize the representation learning; (2) annotating critical parts (He et al. 2019), viewpoint segmentation

(Meng et al. 2020), keypoints and vehicle orientation (Khorramshahi et al. 2019; Wang et al. 2017; Chu et al. 2019) to guide local feature extraction; (3) assembling multiple datasets together (Zheng et al. 2020) or synthesizing vehicle images with rich attributes (Lou et al. 2019; Tang et al. 2019a; Wu et al. 2018) to extend training dataset. In addition, there are a couple of works enhancing ReID models from the perspective of metric learning (Chen et al. 2019b; Chu et al. 2019; Bai et al. 2018; Zhang, Liu, and Zha 2017). Note that vehicle ReID shares many similarities with person ReID for which Ye et al. (2020) conducted a nice survey.

Visual Attention Learning. Many visual attention mechanisms have been proposed, *e.g.*, self-attention (Vaswani et al. 2017), channel attention (Hu, Shen, and Sun 2018) and spatial attention (Woo et al. 2018). Some of them have been introduced into the ReID tasks such as (Chen et al. 2019c,a; Zhou et al. 2019b; Khorramshahi et al. 2019). Chen et al. (2019a) and Zhou et al. (2019b) proposed using attentional gain and multi-level foreground mask consistency to regularize VAL, respectively, while Wang et al. (2020) adopted equivariant constraints for affine transformation in weakly supervised semantic segmentation for the same purpose. He et al. (2019); Meng et al. (2020) proposed training a second attentional branch based on extra part annotations to recognize interest-of-regions for highlighting the part features by weighting global representations with attention masks. Khorramshahi et al. (2019) proposed filtering annotated keypoints under the guidance of vehicle orientation to focus on such keypoint features. A nice survey on VAL can be found in (Chaudhari et al. 2019) and references therein.

Self-Supervised Learning. The success of SSL hinges on devising appropriate pretext task to supervise model learning and a variety of novel tasks have been constructed for, for instance, image generation (Iizuka, Simo-Serra, and Ishikawa 2017), colorization (Zhang, Isola, and Efros 2017), patch position prediction (Doersch, Gupta, and Efros 2015; Kolesnikov, Zhai, and Beyer 2019), patch order classification (Kim, Cho, and Kweon 2019; Kolesnikov, Zhai, and Beyer 2019) and image rotation recognition (Zhai et al. 2019; Feng, Xu, and Tao 2019). Besides, recently contrastive learning of multi-view images (Chen et al. 2020; He et al. 2020) has demonstrated its efficacy. Furthermore, these tasks can also be applied as accompany to improve the performance of the main task in multi-task optimization (Gidaris et al. 2019; Chen et al. 2019d). A nice survey on SSL can be found in (Jing and Tian 2020) and references therein.

In contrast to these previous works, we propose regularizing VAL from the perspective of self-supervision, which has not been explored in the literature. We also propose a new deep learning framework for ReID tasks and demonstrate the SOTA performance on vehicle ReID.

3 Self-Supervised Visual Attention Learning

3.1 Formulation

Given a query image, vehicle ReID aims to predict a ranking list for all gallery images based on the similarity of each pair of query and gallery images. In other words, if two vehicle

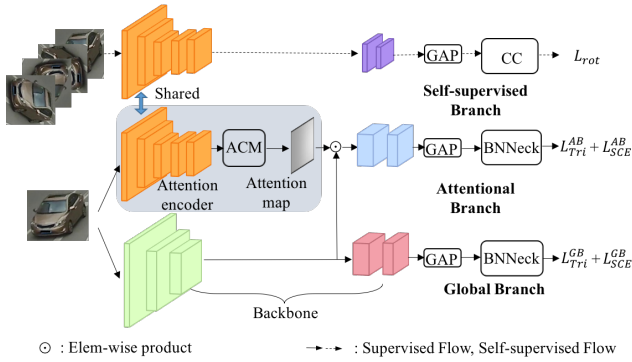


Figure 2: Overview of our network architecture for ReID, including the key components: attention computing module (ACM), batch normalization neck (BNNNeck), cosine classifier (CC), and global average pooling (GAP).

images are more similar semantically, their feature similarity should be larger that leads to a higher rank.

To learn a proper similarity function, we propose a three-branch framework as illustrated in Fig. 2. Specifically, given an image $x \in \mathcal{X}$, these branches can be defined as follows:

- *Global Branch* is our backbone and devised to encode robust codes from the whole input image. Its mapping function can be modeled as

$$F_{GB}(x) = g_{GB}(f_{GB}(x, \alpha_{GB}), \beta_{GB}) \quad (1)$$

where $f_{GB} : \mathcal{X} \rightarrow \mathcal{T}_1$ denotes a function, parametrized by α_{GB} , that maps an image into a feature tensor space \mathcal{T}_1 , and $g_{GB} : \mathcal{T}_1 \rightarrow \mathcal{V}_1$ denotes another function, parametrized by β_{GB} , that maps a feature tensor into a vector space \mathcal{V}_1 .

- *Attentional Branch* is responsible for learning attention maps and producing discriminative features locally. Its mapping function can be modeled as

$$F_{AB}(x) = g_{AB}(f_{GB}(x, \alpha_{GB}) \odot f_{AB}(h(x, \alpha_{AB})), \beta_{AB}) \quad (2)$$

where $h : \mathcal{X} \rightarrow \mathcal{T}_2$ denotes a function, parametrized by α_{AB} , to map an image into another tensor space \mathcal{T}_2 , $f_{AB} : \mathcal{T}_2 \rightarrow \mathcal{M}$ denotes a function to map a feature tensor into an attention mask space \mathcal{M} with the same spatial dimension as \mathcal{T}_1 , $g_{AB} : \mathcal{T}_1 \rightarrow \mathcal{V}_2$ denotes a function, parametrized by β_{AB} , to map a feature tensor into another vector space \mathcal{V}_2 , and \odot denotes the entry-wise multiplication operation.

- *Self-supervised Branch* regularizes its learning of the attentional branch by sharing the attention encoder. Its mapping function can be modeled as

$$F_{SB}(x') = g_{SB}(h(x', \alpha_{AB}), \beta_{SB}) \quad (3)$$

where $g_{SB} : \mathcal{T}_2 \rightarrow \mathcal{V}_3$ is a function, parametrized by β_{SB} , to map a feature tensor into a third vector space \mathcal{V}_3 , and x' denotes a new image by transforming x (e.g., rotation).

Regularization Perspective from Lifting. From Eq. 2 and Eq. 3 we can clearly see that F_{AB}, F_{SB} share a common function h . This indicates that the change of h will have a significant impact on both functions, and vice versa. Therefore, the learning of parameter α_{AB} is controllable by both functions, rather than only F_{AB} in conventional VAL.

In fact, from the same lifting perspective we can easily see that in terms of functionality F_{AB} in Eq. 2 also enforces the regularization on F_{GB} in Eq. 1 through a shared function f_{GB} . Considering the model complexity and data complexity in ReID tasks, such regularization is very important in learning, where the attentional branch plays a key role to connect the other two independent branches smoothly as a bridge. In our experiments, we demonstrate that GB+AB performs better than GB, and GB+AB+SB further improves the performance. Such empirical evidences support our understanding on regularization in learning.

Learning Objective. Given a training set $\{(x_i, y_i)\}_{i \in \mathcal{I}}$ where $(x_i, y_i) \in \mathcal{X} \times \mathcal{Y}, \forall i$ denotes a pair of an image and its ID label, respectively, we denote $s_{ij} = \phi(F_{GB}(x_i), F_{AB}(x_i), F_{GB}(x_j), F_{AB}(x_j))$ as the similarity between images x_i, x_j defined by function ϕ . We then propose optimizing the following problem to learn the model:

$$\begin{aligned} \min_{\alpha, \beta, \gamma} \lambda_1 \sum_{i \in \mathcal{I}} \mathcal{L}_1(F_{GB}(x_i), F_{AB}(x_i), y_i, \gamma_1) \\ + \lambda_2 \sum_{i, j, k \in \mathcal{I}} \mathcal{L}_2(s_{ij}, s_{ik}, y_i, y_j, y_k) \\ + \sum_{i \in \mathcal{I}} \mathcal{L}_3(F_{SB}(x'_i), y'_i, \gamma_2) \end{aligned} \quad (4)$$

where $\alpha = \{\alpha_{GB}, \alpha_{AB}\}, \beta = \{\beta_{GB}, \beta_{AB}, \beta_{SB}\}, \gamma = \{\gamma_1, \gamma_2\}$ denote the learnable parameters, \mathcal{L}_1 denotes an ID loss with parameter γ_1 , \mathcal{L}_2 denotes a triplet loss, \mathcal{L}_3 denotes a self-supervised loss with parameter γ_2 , y'_i denotes pseudo label of x'_i , and $\lambda_1, \lambda_2 \geq 0$ denote two predefined scalars. Note that only the triplet loss \mathcal{L}_2 is defined based on the image similarity to enforce $s_{ij} \geq s_{ik}$ if $y_i = y_j \neq y_k$.

Inference for ReID. Given $\{x_p\}_{p \in \mathcal{P}}, \{x_q\}_{q \in \mathcal{Q}}$ as sets of gallery and query images, respectively, we need to predict a ranking list of x_p 's for every x_q based on the learned similarity function s . We retrieve Top-1 or Top- K gallery images to evaluate our approach using different metrics such as accuracy and mean average precision (mAP).

3.2 Instantiation using Deep Neural Networks

Fig. 2 illustrates an instantiation of our approach using deep learning, where each subnetwork with a unique color represents one of the functions in Eq. 1, Eq. 2, and Eq. 3, and these learnable weights refer to the parameters α, β in Eq. 4. We list the network architectural details as follows:

Attention Computing Module (ACM). We illustrate the ACM in Fig. 3, where $L \in \mathbb{R}^{c \times h \times w}$ defines a 3D tensor feature from a lightweight network similar to D2-Net (Dusmanu et al. 2019), and c, h, w denote the channel, height and width dimension, respectively. Then softmax normalization

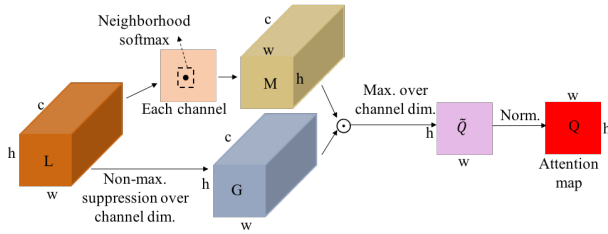


Figure 3: Illustration of attention computing module (ACM).

over neighborhood of each point is conducted along each channel in L , i.e., $M(k, u, v) = \frac{\exp(L(k, u, v))}{\sum_{(m, n) \in \mathcal{N}(u, v)} \exp(L(k, m, n))}$, where $\mathcal{N}(u, v)$ denotes neighborhood set with size \mathcal{K} around location (u, v) along the k -th channel. Meanwhile, non-maximum suppression across all the channels is conducted in L as well, i.e., $G(k, u, v) = \frac{L(k, u, v)}{\max_{t=1, \dots, c} L(t, u, v)}$. To amplify the informative signal effectively, we obtain our soft mask Q by $Q(u, v) = \frac{\tilde{Q}(u, v)}{\sum_{(m, n)} \tilde{Q}(m, n)}$ where $\tilde{Q}(u, v) = \max_{t=1, \dots, c} \{M(t, u, v) \cdot G(t, u, v)\}$.

Batch Normalization Neck (BNNeck). Luo et al. (2019) proposed this network for ReID by adding a batch normalization layer (BN) without bias term between the GAP and the fully connected (FC) layer as well as removing bias term in FC. Empirically it was demonstrated that BNNeck can improve the inconsistency between the triplet loss and the ID loss during training, leading to better generalization.

Self-Supervised Branch. In general, SSL is equivalent to supervised learning with pseudo labels, and often taken as an auxiliary task together with the original learning task. Motivated by recent works such as (Feng, Xu, and Tao 2019; Kolesnikov, Zhai, and Beyer 2019), we propose using image rotation degrees as pseudo labels for prediction based on the cosine classifier (CC) (Gidaris et al. 2019; Wojke and Bewley 2018). Specifically, to prepare the auxiliary data and labels, we rotate each training image by 0° , 90° , 180° or 270° and assign 0, 1, 2 or 3 as its pseudo label accordingly.

Other Architectural Details. Same as most of the ReID works, we choose ResNet50 (He et al. 2016) as our model backbone, with $stride = 2$ in $conv5_x$ replaced with $stride = 1$ to output larger feature maps (Chen et al. 2019c; Luo et al. 2019). In the *Global Branch*, the backbone is divided into two phases: the first phase ($conv1$, $conv2_x$, $conv3_x$) and second phase ($conv4_x$, $conv5_x$). In the *Attentional Branch*, ResNet18 is modified as the attention encoder by setting $stride = 1$ in $conv4_x$, $conv5_x$ to extract local features. By passing through it, each image is only downsampled by 8 times so that attention can be computed in a larger space. Then the local discriminative features after entry-wise multiplication are fed into $conv4_x'$, $conv5_x'$, holding identical architectures with $conv4_x$, $conv5_x$ in ResNet50, for further process. In the *Self-supervised Branch*, the features from the shared sub-network are fed into another sub-network consisting of two basic blocks (He et al. 2016) (with $stride = 2$ in the first

convolutional layer).

3.3 Training & Testing

To train our network, we utilize the hard mining triplet loss (Tri) (Hermans, Beyer, and Leibe 2017) and the smoothed cross-entropy (SCE) loss (Szegedy et al. 2016) that are widely used in the ReID tasks. We also choose the negative Euclidean distance as our similarity measure.

Implicit Data Augmentation in Training. To better explain this, we list the hard mining triplet loss as below:

$$\mathcal{L}_{Tri}(x, \mathcal{X}_{PN}) = \left[\tau - \min_{p=1, \dots, P} s(F(x), F(x_p)) + \max_{n=1, \dots, N} s(F(x), F(x_n)) \right]_+ \quad (5)$$

where x denotes an image, $\{x_p\} \subseteq \mathcal{X}_{PN}$ denote the positive image set with the same ID as x , $\{x_n\} \subseteq \mathcal{X}_{PN}$ denote the negative image set with different IDs, s denotes the similarity function, F denotes the feature extraction function, and $[\cdot]_+$ denotes the nonnegative operator with a constant margin τ . Note that this loss aims to maximize the margin between minimum positive similarity and maximum negative similarity for better discriminability among features.

In our network training, we propose applying this triplet loss, as well as the SCE loss, to the global branch and the attentional branch separately, rather than taking the concatenation of F_{GB}, F_{AB} as a feature vector F for training. In this way, there is much more flexibility in choosing the positive and negative pairs for both branches in the loss that can come from different images. Such image mixture from both branches allows our training to exploit more ‘‘images’’ implicitly for better generalization.

Finally we define our overall loss function as

$$\mathcal{L}_{overall} = \lambda_{Tri}^{GB} \mathcal{L}_{Tri}^{GB} + \lambda_{SCE}^{GB} \mathcal{L}_{SCE}^{GB} + \lambda_{Tri}^{AB} \mathcal{L}_{Tri}^{AB} + \lambda_{SCE}^{AB} \mathcal{L}_{SCE}^{AB} + \lambda_{rot} \mathcal{L}_{rot}, \quad (6)$$

where \mathcal{L}_{rot} denotes the CE loss based on the cosine classifier for the self-supervised branch. To avoid heavy tuning of the hyperparameters, we simply set λ_{Tri}^{GB} , λ_{SCE}^{GB} , λ_{Tri}^{AB} , λ_{SCE}^{AB} to 0.5 and λ_{rot} to 1.0 in all the experiments. Only λ_{rot} is fine-tuned in our ablation study.

ReID Testing. At the test stage, the self-supervised branch is deactivated for inference. Following the suggestions in (Luo et al. 2019), we normalize the concatenation vector of F_{GB}, F_{AB} for each image as the feature vector, and use the Euclidean distance for ranking. In fact, similar to (Luo et al. 2019), we observe that empirically such ℓ_2 -normalized features can improve the performance by $\sim 1\%$ over different combinations of training and testing approaches, including training with the feature concatenation. In our experiments, we report the performance of the network in Fig. 2 using the normalized features.

4 Experiments

Datasets. We conduct comprehensive experiments on three benchmark datasets for vehicle ReID. *VeRi-776* (Liu et al.

2016b) contains 49,357 multi-view images of 776 vehicles and 37,778 images of 576 identities are chosen as training set, the rest as test set. *CityFlow-ReID* (Tang et al. 2019b) is a challenging dataset where images are captured by 40 cameras under diverse environments. 36,935 images from 333 identities form the training set and the testing set contains 18,290 images from the other 333 vehicles. *VehicleID* (Liu et al. 2016a) is a large-scale benchmark containing 221,763 images of 26,267 vehicles. All images are taken from front or rear view. The gallery set only contains one randomly selected image for each testing identity, and thus here we report our results as the mean over 10 trials. In this dataset there are three numbers of gallery images widely used for testing, *i.e.*, 800 (small), 1600 (medium) and 2400 (large).

Training & Evaluation Protocols. During training, random cropping, horizontally flipping and erasing are performed as data augmentation strategies. None of them is adopted to process testing images. All images are resized to 256×256 . We choose PyTorch to implement our model and adopt Adam optimizer (Kingma and Ba 2014) with default betas ($\beta_1 = 0.9$, $\beta_2 = 0.999$), weight decay $5e-4$ to optimize it. All experiments are conducted on one NVIDIA GEFORCE RTX 2080Ti GPU. The training batch size on VeRi-776 and CityFlow-ReID is 28 and on VehicleID is 40 with 4 images from each instance. On VeRi-776 and CityFlow-ReID, the initial learning rate is $1e-4$ and the margin of triplet loss is set as $\tau = 0.5$ empirically. The number of training epochs is 80 and the learning rate decreases by multiplying 0.1 at epoch 20, 40, 60, respectively. On VehicleID, the margin is $\tau = 0.7$ and the number of learning epochs is 120. The learning rate increases linearly from 0 to $1e-4$ during the first 10 epochs, decreases by cosine scheduler to $1e-7$ at 100th epoch and to 0 at the last epoch.

At test time we evaluate our approach using 4 widely used metrics in the ReID tasks, *i.e.*, image-to-track retrieval mAP (tmAP) if tracks are available in the data, image-to-image retrieval mAP (imAP), Top-1 and Top-5 accuracy. We show these metric numbers as percentages and the best are marked in bold. Following the literature of ReID, *e.g.*, (Meng et al. 2020; He et al. 2019; Chen et al. 2019c), we report our best performance on each dataset with no cross-validation.

4.1 State-of-the-art Performance Comparison

VeRi-776. We list our comparison results in Table 1 with recent SOTA algorithms, *i.e.*, Siamese+Path (Shen et al. 2017), OIFE and OIFE+ST (Wang et al. 2017), VAMI (Zhou and Shao 2018), NuFACT (Liu et al. 2017), AAVER (Khorramshahi et al. 2019), RS and R+MT+K (Tang et al. 2019a), VANet (Chu et al. 2019), SAN (Qian et al. 2020a), PART (He et al. 2019), PVEN (Meng et al. 2020), DMML (Chen et al. 2019b). We can see that most of recent methods utilized extra labels. For instance, VANet annotated 5,000 images from VeRi-776 and VehicleID, respectively, to train a viewpoint predictor and learned distinct metrics for similar or dissimilar viewpoint pairs. AAVER relied on predefined keypoint and orientation prediction to guide the learning of discriminative features. Also, SAN adopted various attribute labels to supervise its attribute-aware branch. Besides, PART

Method	EI	tmAP	imAP	Top-1	Top-5
Siamese+Path	Y	58.27	-	83.49	90.04
OIFE	Y	48.0	-	65.9	87.7
OIFE+ST	Y	51.42	-	68.3	89.7
VAMI	Y	50.13	-	77.03	90.82
NuFACT	Y	53.42	-	81.56	95.11
AAVER	Y	58.52	-	88.68	94.10
RS	Y	-	63.76	90.70	94.40
R+MT+K	Y	-	65.44	90.94	96.72
VANet	Y	66.34	-	89.78	95.99
SAN	Y	72.5	-	93.3	97.1
PART	Y	74.3	-	94.3	98.7
PVEN	Y	-	79.5	95.6	98.4
DMML	N	-	70.1	91.2	96.3
Ours	N	86.2	80.9	95.9	98.2

Table 1: Result comparison on VeRi-776, where EI is short for extra information for stronger supervision in learning.

Method	EI	imAP	Top-1	Top-5
FVS	Y	5.08	20.82	24.52
RS	Y	25.66	50.37	61.48
R+MT+K	Y	30.57	54.56	66.54
Xent	N	18.62	39.92	52.66
Htri	N	24.04	45.75	61.24
Cent	N	9.49	27.92	39.77
Xent+Htri	N	25.06	51.69	62.84
BA	N	25.61	49.62	65.02
BS	N	25.57	49.05	63.12
Ours	N	37.14	60.08	67.21

Table 2: Result comparison on CityFlow-ReID.

defined three types of vehicle parts, *i.e.*, front and back lights, front and back windows, and vehicle brand, as objects to optimize YOLO in an offline manner. When training the ReID model, they extracted local features from detected locations by YOLO as supplementary information for global representations. In PVEN, they provided part segmentation ground-truth based on viewpoint visibility for 3,165 images from VeRi-776 to train a U-Net parser. They implemented part-aware feature alignment using the mask produced from the segmentor. In contrast, our model does not need any additional annotations to assist local feature learning. Although, due to GPU limitation, our training batch size 28 on VeRi-776 is much smaller than other methods (*e.g.*, 256 in SAN), our method can still outperform the other competitors significantly in terms of tmAP, imAP and Top-1 accuracy. On Top-5 accuracy ours is only 0.5% lower than the best that uses image size of 512×512 for training.

CityFlow-ReID. We compare our method with FVS (Tang et al. 2018), RS and R+MT+K (Tang et al. 2019a), Xent, Htri, Cent and Xent+Htri (Zhou and Xiang 2019), BA and BS (Kuma et al. 2019) in Table 2. This dataset is very challenging because images are taken from 5 scenarios, covering a diverse set of location types, various scenes and traffic

Method	EI	Small		Medium		Large	
		Top-1	Top-5	Top-1	Top-5	Top-1	Top-5
MD+CCL	Y	49.0	73.5	42.8	66.8	38.2	61.6
OIFE	Y	-	-	-	-	67.0	82.9
VAMI	Y	63.1	83.3	52.9	75.1	47.3	70.3
GoogLeNet	Y	47.90	67.43	43.45	63.53	38.24	59.51
NuFACT	Y	48.90	69.51	43.64	65.34	38.63	60.72
AAVER	Y	72.47	93.22	66.85	89.39	60.23	84.85
VANet	Y	88.12	97.29	83.17	95.14	80.35	92.97
SAN	Y	79.7	94.3	78.4	91.3	75.6	88.3
PART	Y	78.4	92.3	75.0	88.3	74.2	86.4
PVEN	Y	84.7	97.0	80.6	94.5	77.8	92.0
Ours	N	86.8	97.4	83.5	95.6	80.8	93.7

Table 3: Results comparison on VehicleID.

Method	VeRi-776		CityFlow-ReID	
	tmAP	imAP	imAP	Top-1
GB w/o attention	84.0	78.3	32.04	56.27
GB+ResNet18 w/o attention	85.2	79.5	34.63	57.98
GB+AB ($\mathcal{K} = 7$)	<u>85.9</u>	<u>80.7</u>	<u>36.63</u>	<u>59.98</u>
GB+AB ($\mathcal{K} = 11$)	85.8	80.6	35.94	59.70
GB+AB ($\mathcal{K} = 15$)	85.5	80.2	36.32	58.56
GB+AB+SB ($\lambda_{rot} = 0.1$)	85.8	80.5	36.61	59.13
GB+AB+SB ($\lambda_{rot} = 1.0$)	86.2	80.9	37.14	60.08
GB+AB+SB ($\lambda_{rot} = 2.0$)	86.1	80.9	36.54	59.60
GB+AB+SB ($\lambda_{rot} = 3.0$)	85.9	80.7	36.89	60.36
GB+AB+SB ($\lambda_{rot} = 10.0$)	85.9	80.5	36.54	59.13

Table 4: Experimental results for our ablation study, where we underline the selected parameters for \mathcal{K} in ACM and λ_{rot} in Eq. 6. The performance improvement upon each component is observed consistently across the datasets.

conditions. Results of metric learning methods (Xent, Htri, Cent, Xent+Htri) and batch-based sampling methods (BA, BS) are acquired with no using extra annotations. In terms of extra information, in RS real and synthetic vehicle images were exploited, while R+MT+K employed keypoint coordinates, vehicle types and color labels to perform multi-task learning and conduct pose estimation based ReID. As we see in Table 2, our approach achieves the best performance on all the three metrics (no tmAP comparison because of no track data available), with no any extra annotation.

VehicleID. Current SOTA methods on this dataset are identical to those on VeRi-776, except MD+CCL (Liu et al. 2016a) and GoogLeNet (Yang et al. 2015), and we list all the comparison results in Table 3. Different from ours, VANet and PVEN utilized larger batch sizes of 128 and 256, respectively. Even so, our approach still can beat all the other competitors in almost all the settings.

4.2 Ablation Study

In order to evaluate the effect of each branch in our network on the performance comprehensively, we conduct extensive experiments on VeRi-776 and CityFlow-ReID. Here we re-

port tmAP and imAP on VeRi-776 and imAP and Top-1 on CityFlow-ReID, because these metrics are more important on each dataset. We list our results in Tabel 4.

Larger Networks as Backbone in GB without Attention.

Compared with GB alone, our network has another extra attentional branch plus self-supervised branch, making the network larger. To see the effect of different networks as backbone with no attention, we implement a new network consisting of two independent branches, one ResNet50 and one ResNet18, whose output features are concatenated for ReID testing. We denote this network as ‘‘GB+ResNet18 w/o attention’’ in the table. We can see that the performance can be marginally beneficial from a larger backbone as a global branch. This also indicates that our results still have room for improvement, but for the demonstration purpose we choose to use a simpler backbone.

AB Improvement over GB with Neighborhood Size \mathcal{K} in ACM.

We conduct three experiments with different \mathcal{K} to explore the effect of neighborhood size on the performance while fixing the other hyperparameters. Note that such attention operations are conducted on 8x downsampled feature maps rather than the original image size whose actual receptive field is $64\mathcal{K}^2$. Compared with the baseline using GB alone, we can see substantial improvements on all the metrics, especially for the challenging CityFlow-ReID dataset. Such improvements are relatively robust *w.r.t.* \mathcal{K} , and we set $\mathcal{K} = 7$ by default in our experiments. Note that by comparing ‘‘GB+AB’’ with ‘‘GB+ResNet18 w/o attention’’ we can conclude that a good attention mechanism is much more important than a similar larger backbone in GB.

Further Improvement from SB with Tradeoff Parameter λ_{rot} .

To choose a proper coefficient for the self-supervised loss \mathcal{L}_{rot} , we evaluate λ_{rot} within different scales to perform comparison while fixing the other hyperparameters. It is clear that self-supervised learning with $\lambda_{rot} = 1.0$ boosts ReID performance further on all the metrics across both datasets. Again the small performance fluctuations with largely different λ_{rot} suggest the robustness of our method.

It is worth mentioning that such performance improvements from either AB or SB or both essentially come from our attention mechanism that helps regularize GB as well as AB, leading to significantly better generalization in the training of our network.

4.3 Attention Visualization

Our self-supervised visual attention learning aims to capture discriminative local features by assigning large weights around detected key parts. To verify this, we visualize our attentional masks in Fig. 4 by upsampling the attention maps by 8x and then overlaying them on the corresponding input images. As expected, our attention mechanism can consistently locate discriminative features such as wheels and licence plates for the same vehicle instance from different views across different cameras. This is the key to the success of our approach in vehicle ReID.



Figure 4: Visualization of learned attention masks on **(top)** VeRi-776 and **(bottom)** CityFlow-ReID. Each row represents the images from the same instance.

4.4 Generalization to Other ReID Tasks

In this section we will demonstrate the potentials of using our approach in person ReID and multi-target multi-camera (MTMC) tracking that are highly related to vehicle ReID.

Person ReID. Rather than identifying individual vehicles, this task aims to identify the same person in images from different cameras. We conduct some experiments on Market-1501 (Zheng et al. 2015), a widely used benchmark dataset for person ReID. Our training details keep identical to those on VehicleID. Our approach can achieve 86.1%, 94.3% and 98.3% in terms of imAP, Top-1 and Top-5 accuracy, respectively, which are comparable or even better than recent methods (Zheng et al. 2019; Zhou et al. 2019a). We also visualize the learned attention masks in Fig. 5. Surprisingly, with no extra labels of body parts, our approach can manage to consistently align the masks well with the body parts such as head, arms and legs, similar to our observations in Fig. 4.

MTMC Tracking. Given the tracklets of multiple targets in the videos from different cameras, this task aims to synchronize such tracklets with the same target across the cameras, *i.e.*, ReID with tracklets rather than images. We conduct our experiments on the dataset used in City-Scale Multi-Camera Vehicle Tracking in AI City Challenge 2020 (Tang et al. 2019c). Similar to (Qian et al. 2020b), we simply adopt an



Figure 5: Visualization of learned attention masks for person ReID on Market-1501. Each group of three images horizontally are from the same person.

Rank	1	2	3	4	5	6
Team ID	Ours	92	141	11	163	63
IDF1 Score	0.4930	0.4616	0.4552	0.4400	0.4369	0.3677

Table 5: Performance comparison in the leaderboard of city-scale multi-camera vehicle tracking in AI City Challenge 2020. See <https://www.aicitychallenge.org> for more details.

efficient MTMC tracking pipeline. Specifically, we firstly use the pre-trained Mask R-CNN (He et al. 2017) to detect vehicles from each video frame. Then we use Deep SORT (Wojke, Bewley, and Paulus 2017) with association strategy from (Wang et al. 2019) to perform online multi-target single camera vehicle tracking. Now we directly apply our vehicle ReID model pre-trained on VeRi-776 (with visible license plates) without fine-tuning to synchronize such separate tracklets by re-identifying the vehicle instance of each tracklet across multi-camera videos. We list our comparison in Table 5 where, as of writing this paper, our result achieves rank 1 in the leaderboard that is significantly better than the second best.

In summary, we believe that our approach can be well generalized to other ReID tasks, with the capability of consistently locating discriminative features for the same instance across different scenarios using attention masks.

5 Conclusion

In this paper we propose a novel deep learning framework for vehicle ReID by learning the visual attention masks for generating discriminative features, both globally and locally. We introduce self-supervised learning (SSL) to better regularize the visual attention learning (VAL) through a shared function in lifting. Based on this, we propose an effective instantiation using deep neural networks that consists of global, attentional and self-supervised branches. We evaluate it on three benchmarks for vehicle ReID. Our results can always achieve comparable to, or even better than, the current SOTA. We also generalize our approach to other ReID related tasks such as person ReID and multi-target multi-camera tracking with good performances. Visualization verifies the effectiveness of our attention masks.

References

- Bai, Y.; Lou, Y.; Gao, F.; Wang, S.; Wu, Y.; and Duan, L.-Y. 2018. Group-sensitive triplet embedding for vehicle re-identification. *IEEE Transactions on Multimedia* 20(9): 2385–2399.
- Chaudhari, S.; Polatkan, G.; Ramanath, R.; and Mithal, V. 2019. An attentive survey of attention models. *arXiv preprint arXiv:1904.02874*.
- Chen, G.; Lin, C.; Ren, L.; Lu, J.; and Zhou, J. 2019a. Self-Critical Attention Learning for Person Re-Identification. In *ICCV*.
- Chen, G.; Zhang, T.; Lu, J.; and Zhou, J. 2019b. Deep Meta Metric Learning. In *ICCV*.
- Chen, T.; Ding, S.; Xie, J.; Yuan, Y.; Chen, W.; Yang, Y.; Ren, Z.; and Wang, Z. 2019c. ABD-Net: Attentive but Diverse Person Re-Identification. In *ICCV*.
- Chen, T.; Kornblith, S.; Norouzi, M.; and Hinton, G. 2020. A simple framework for contrastive learning of visual representations. *arXiv preprint arXiv:2002.05709*.
- Chen, T.; Zhai, X.; Ritter, M.; Lucic, M.; and Houthsby, N. 2019d. Self-supervised gans via auxiliary rotation loss. In *CVPR*, 12154–12163.
- Chu, R.; Sun, Y.; Li, Y.; Liu, Z.; Zhang, C.; and Wei, Y. 2019. Vehicle re-identification with viewpoint-aware metric learning. In *ICCV*, 8282–8291.
- Doersch, C.; Gupta, A.; and Efros, A. A. 2015. Unsupervised visual representation learning by context prediction. In *ICCV*, 1422–1430.
- Dusmanu, M.; Rocco, I.; Pajdla, T.; Pollefeys, M.; Sivic, J.; Torii, A.; and Sattler, T. 2019. D2-Net: A Trainable CNN for Joint Description and Detection of Local Features. In *CVPR*.
- Feng, Z.; Xu, C.; and Tao, D. 2019. Self-supervised representation learning by rotation feature decoupling. In *CVPR*, 10364–10374.
- Fu, J.; Liu, J.; Tian, H.; Li, Y.; Bao, Y.; Fang, Z.; and Lu, H. 2019. Dual Attention Network for Scene Segmentation. In *CVPR*.
- Gidaris, S.; Bursuc, A.; Komodakis, N.; Pérez, P.; and Cord, M. 2019. Boosting few-shot visual learning with self-supervision. In *ICCV*, 8059–8068.
- Guo, H.; Zhu, K.; Tang, M.; and Wang, J. 2019. Two-level attention network with multi-grain ranking loss for vehicle re-identification. *IEEE Transactions on Image Processing* 28(9): 4328–4338.
- He, B.; Li, J.; Zhao, Y.; and Tian, Y. 2019. Part-Regularized Near-Duplicate Vehicle Re-Identification. In *CVPR*.
- He, K.; Fan, H.; Wu, Y.; Xie, S.; and Girshick, R. 2020. Momentum contrast for unsupervised visual representation learning. In *Proceedings of the IEEE/CVF Conference on Computer Vision and Pattern Recognition*, 9729–9738.
- He, K.; Gkioxari, G.; Dollár, P.; and Girshick, R. 2017. Mask r-cnn. In *ICCV*, 2961–2969.
- He, K.; Zhang, X.; Ren, S.; and Sun, J. 2016. Deep residual learning for image recognition. In *CVPR*, 770–778.
- Hermans, A.; Beyer, L.; and Leibe, B. 2017. In defense of the triplet loss for person re-identification. *arXiv preprint arXiv:1703.07737*.
- Hu, J.; Shen, L.; and Sun, G. 2018. Squeeze-and-excitation networks. In *CVPR*, 7132–7141.
- Iizuka, S.; Simo-Serra, E.; and Ishikawa, H. 2017. Globally and locally consistent image completion. *ACM Transactions on Graphics (ToG)* 36(4): 1–14.
- Jing, L.; and Tian, Y. 2020. Self-supervised visual feature learning with deep neural networks: A survey. *IEEE Transactions on Pattern Analysis and Machine Intelligence*.
- Khorramshahi, P.; Kumar, A.; Peri, N.; Rambhatla, S. S.; Chen, J.-C.; and Chellappa, R. 2019. A dual-path model with adaptive attention for vehicle re-identification. In *ICCV*, 6132–6141.
- Kim, D.; Cho, D.; and Kweon, I. S. 2019. Self-supervised video representation learning with space-time cubic puzzles. In *Proceedings of the AAAI Conference on Artificial Intelligence*, volume 33, 8545–8552.
- Kingma, D. P.; and Ba, J. 2014. Adam: A method for stochastic optimization. *arXiv preprint arXiv:1412.6980*.
- Kolesnikov, A.; Zhai, X.; and Beyer, L. 2019. Revisiting Self-Supervised Visual Representation Learning. In *CVPR*.
- Kuma, R.; Weill, E.; Aghdasi, F.; and Sriram, P. 2019. Vehicle re-identification: an efficient baseline using triplet embedding. In *2019 International Joint Conference on Neural Networks (IJCNN)*, 1–9. IEEE.
- Liu, H.; Tian, Y.; Wang, Y.; Pang, L.; and Huang, T. 2016a. Deep Relative Distance Learning: Tell the Difference Between Similar Vehicles. In *CVPR*, 2167–2175.
- Liu, X.; Liu, W.; Mei, T.; and Ma, H. 2016b. A deep learning-based approach to progressive vehicle re-identification for urban surveillance. In *European conference on computer vision*, 869–884. Springer.
- Liu, X.; Liu, W.; Mei, T.; and Ma, H. 2017. Provid: Progressive and multimodal vehicle re-identification for large-scale urban surveillance. *IEEE Transactions on Multimedia* 20(3): 645–658.
- Liu, X.; Zhang, S.; Huang, Q.; and Gao, W. 2018. Ram: a region-aware deep model for vehicle re-identification. In *2018 IEEE International Conference on Multimedia and Expo (ICME)*, 1–6. IEEE.
- Lou, Y.; Bai, Y.; Liu, J.; Wang, S.; and Duan, L.-Y. 2019. Embedding adversarial learning for vehicle re-identification. *IEEE Transactions on Image Processing* 28(8): 3794–3807.
- Luo, H.; Jiang, W.; Gu, Y.; Liu, F.; Liao, X.; Lai, S.; and Gu, J. 2019. A Strong Baseline and Batch Normalization Neck for Deep Person Re-identification. *IEEE Transactions on Multimedia*.
- Meng, D.; Li, L.; Liu, X.; Li, Y.; Yang, S.; Zha, Z.-J.; Gao, X.; Wang, S.; and Huang, Q. 2020. Parsing-based View-aware Embedding Network for Vehicle Re-Identification. In

- Proceedings of the IEEE/CVF Conference on Computer Vision and Pattern Recognition*, 7103–7112.
- Qian, J.; Jiang, W.; Luo, H.; and Yu, H. 2020a. Stripe-based and attribute-aware network: A two-branch deep model for vehicle re-identification. *Measurement Science and Technology*.
- Qian, Y.; Yu, L.; Liu, W.; and Hauptmann, A. G. 2020b. ELECTRICITY: An efficient multi-camera vehicle tracking system for intelligent city. In *Proceedings of the IEEE/CVF Conference on Computer Vision and Pattern Recognition Workshops*, 588–589.
- Shen, Y.; Xiao, T.; Li, H.; Yi, S.; and Wang, X. 2017. Learning deep neural networks for vehicle re-id with visual-spatio-temporal path proposals. In *ICCV*, 1900–1909.
- Szegedy, C.; Vanhoucke, V.; Ioffe, S.; Shlens, J.; and Wojna, Z. 2016. Rethinking the inception architecture for computer vision. In *CVPR*, 2818–2826.
- Tang, Z.; Naphade, M.; Birchfield, S.; Tremblay, J.; Hodge, W.; Kumar, R.; Wang, S.; and Yang, X. 2019a. Pamtri: Pose-aware multi-task learning for vehicle re-identification using highly randomized synthetic data. In *ICCV*, 211–220.
- Tang, Z.; Naphade, M.; Liu, M.-Y.; Yang, X.; Birchfield, S.; Wang, S.; Kumar, R.; Anastasiu, D.; and Hwang, J.-N. 2019b. Cityflow: A city-scale benchmark for multi-target multi-camera vehicle tracking and re-identification. In *CVPR*, 8797–8806.
- Tang, Z.; Naphade, M.; Liu, M.-Y.; Yang, X.; Birchfield, S.; Wang, S.; Kumar, R.; Anastasiu, D.; and Hwang, J.-N. 2019c. CityFlow: A City-Scale Benchmark for Multi-Target Multi-Camera Vehicle Tracking and Re-Identification. In *CVPR*.
- Tang, Z.; Wang, G.; Xiao, H.; Zheng, A.; and Hwang, J.-N. 2018. Single-camera and inter-camera vehicle tracking and 3D speed estimation based on fusion of visual and semantic features. In *CVPR Workshops*, 108–115.
- Vaswani, A.; Shazeer, N.; Parmar, N.; Uszkoreit, J.; Jones, L.; Gomez, A. N.; Kaiser, Ł.; and Polosukhin, I. 2017. Attention is all you need. In *NeurIPS*, 5998–6008.
- Wang, Y.; Zhang, J.; Kan, M.; Shan, S.; and Chen, X. 2020. Self-supervised Equivariant Attention Mechanism for Weakly Supervised Semantic Segmentation. *arXiv preprint arXiv:2004.04581*.
- Wang, Z.; Tang, L.; Liu, X.; Yao, Z.; Yi, S.; Shao, J.; Yan, J.; Wang, S.; Li, H.; and Wang, X. 2017. Orientation invariant feature embedding and spatial temporal regularization for vehicle re-identification. In *ICCV*, 379–387.
- Wang, Z.; Zheng, L.; Liu, Y.; and Wang, S. 2019. Towards real-time multi-object tracking. *arXiv preprint arXiv:1909.12605*.
- Wojke, N.; and Bewley, A. 2018. Deep cosine metric learning for person re-identification. In *2018 IEEE winter conference on applications of computer vision (WACV)*, 748–756. IEEE.
- Wojke, N.; Bewley, A.; and Paulus, D. 2017. Simple on-line and realtime tracking with a deep association metric. In *2017 IEEE international conference on image processing (ICIP)*, 3645–3649. IEEE.
- Woo, S.; Park, J.; Lee, J.-Y.; and So Kweon, I. 2018. Cbam: Convolutional block attention module. In *Proceedings of the European conference on computer vision (ECCV)*, 3–19.
- Wu, F.; Yan, S.; Smith, J. S.; and Zhang, B. 2018. Joint semi-supervised learning and re-ranking for vehicle re-identification. In *2018 24th International Conference on Pattern Recognition (ICPR)*, 278–283. IEEE.
- Yan, K.; Tian, Y.; Wang, Y.; Zeng, W.; and Huang, T. 2017. Exploiting multi-grain ranking constraints for precisely searching visually-similar vehicles. In *ICCV*, 562–570.
- Yang, L.; Luo, P.; Change Loy, C.; and Tang, X. 2015. A large-scale car dataset for fine-grained categorization and verification. In *CVPR*, 3973–3981.
- Ye, M.; Shen, J.; Lin, G.; Xiang, T.; Shao, L.; and Hoi, S. C. 2020. Deep learning for person re-identification: A survey and outlook. *arXiv preprint arXiv:2001.04193*.
- Zhai, X.; Oliver, A.; Kolesnikov, A.; and Beyer, L. 2019. S4L: Self-Supervised Semi-Supervised Learning. In *ICCV*.
- Zhang, R.; Isola, P.; and Efros, A. A. 2017. Split-brain autoencoders: Unsupervised learning by cross-channel prediction. In *CVPR*, 1058–1067.
- Zhang, Y.; Liu, D.; and Zha, Z.-J. 2017. Improving triplet-wise training of convolutional neural network for vehicle re-identification. In *2017 IEEE International Conference on Multimedia and Expo (ICME)*, 1386–1391. IEEE.
- Zheng, L.; Shen, L.; Tian, L.; Wang, S.; Wang, J.; and Tian, Q. 2015. Scalable person re-identification: A benchmark. In *Proceedings of the IEEE international conference on computer vision*, 1116–1124.
- Zheng, Z.; Ruan, T.; Wei, Y.; Yang, Y.; and Mei, T. 2020. VehicleNet: Learning Robust Visual Representation for Vehicle Re-identification. *arXiv preprint arXiv:2004.06305*.
- Zheng, Z.; Yang, X.; Yu, Z.; Zheng, L.; Yang, Y.; and Kautz, J. 2019. Joint discriminative and generative learning for person re-identification. In *IEEE Conference on Computer Vision and Pattern Recognition (CVPR)*.
- Zhou, K.; and Xiang, T. 2019. Torchreid: A Library for Deep Learning Person Re-Identification in Pytorch. *arXiv preprint arXiv:1910.10093*.
- Zhou, K.; Yang, Y.; Cavallaro, A.; and Xiang, T. 2019a. Omni-scale feature learning for person re-identification. In *ICCV*, 3702–3712.
- Zhou, S.; Wang, F.; Huang, Z.; and Wang, J. 2019b. Discriminative Feature Learning With Consistent Attention Regularization for Person Re-Identification. In *ICCV*, 8040–8049.
- Zhou, Y.; and Shao, L. 2018. Viewpoint-Aware Attentive Multi-View Inference for Vehicle Re-Identification. In *CVPR*.